# Tyre pyrolytic oil blends in a state-of-the-art compression ignition engine: Towards fuel-optimised combustion

# Tyre pyrolytic oil blends in a state-of-the-art compression ignition engine: towards fuel-optimised combustion

Jacek Hunicz[1], Maciej Mikulski[2], Arkadiusz Rybak[1]

1. Lublin University of Technology, Faculty of Mechanical Engineering, Nadbystrzycka 36, 20-618 Lublin, Poland; email: j.hunicz@pollub.pl
2. University of Vaasa, School of Technology and Innovation, Wolffintie 34, FI-65200 Vaasa, Finland; email: maciej.mikulski@uwasa.fi

Corresponding author: Jacek Hunicz, j.hunicz@pollub.pl

## Abstract

The end-to-end efficiency and environmental impact of tyre pyrolysis oil (TPO) are currently high on the agenda of worldwide research. However, most knowledge regarding combustion and emissions of TPO fuels comes from legacy (pre-Euro standard) engine platforms, operating in non-optimal combustion conditions. The few tests on modern automotive engines have used factory, diesel-optimised calibration maps and focus on only small TPO admixtures to diesel fuel (DF). The present work aspires to tackle these knowledge gaps by testing higher TPO admixture diesel blends in a state-of-the-art research engine realising low nitrogen oxides ($NO_X$), partially premixed compression ignition. Measurement campaigns focus on accuracy in establishing fuel-to-fuel differences in emissions, also with consideration of unlegislated species. A combination of thorough combustion analysis and accurate fuel property characterisation allows evaluation of a calibration strategy that harnesses multi-pulse injection and a fully controlled air-path to mitigate emissions. This strategy enables an engine fuelled with a 40% TPO blend to realise low-temperature combustion in a wider area of the calibration map than is possible with DF. The most favourable $NO_X$/particulate matter (PM) mode is extended towards high exhaust gas recirculation and early injection regimes. Adopting this dedicated engine control for

TPO allows best-point $NO_X$/PM emissions of 1.22 g/kWh and 0.18 g/kWh respectively, while maintaining the baseline indicated thermal efficiency target of 42%. Carbon monoxide and hydrocarbons emissions are elevated, but in terms of current EU Non-road Mobile Machinery Stage V limits, differences between TPO and DF are insignificant. However, regardless of calibration, TPO´s chemical make-up causes increased emissions of sulphur oxides and aromatic hydrocarbons.

**Keywords:** tyre pyrolysis oil, premixed compression ignition, engine calibration, emissions, detailed emission speciation

## Nomenclature

| | |
|---|---|
| BMEP | Brake mean effective pressure |
| CA50 | Crank angle at 50% fuel burnt |
| CaO | Calcium oxide |
| $Ca(OH)_2$ | Calcium hydroxide |
| CAD | Crank angle degree |
| CO | Carbon monoxide |
| $CO_2$ | Carbon dioxide |
| CR | Common rail |
| DF | Diesel fuel |
| EGR | Exhaust gas recirculation |
| FAME | Fatty acid methyl esters |
| FTIR | Fourier-transform infrared |
| GC/MS | Gas chromatography/mass spectrometry |
| HC | Unburnt hydrocarbons |
| HRR | Heat release rate |
| HVO | Hydrotreated vegetable oil |

| | |
|---|---|
| ITE | Indicated thermal efficiency |
| IMEP | Indicated mean effective pressure |
| MAP | Manifold absolute pressure |
| MFB | Mass fraction burnt |
| $NO_X$ | Oxides of nitrogen |
| NRMM | Non-road Mobile Machinery |
| PM | Particulate matter |
| PPCI | Partially-premixed compression ignition |
| SOI | Start of injection |
| $SOI_m$ | Start of injection (main injection) |
| $SOI_p$ | Start of injection (pilot injection) |
| TDC | Top dead centre |
| TPO | Tyre pyrolysis oil |

## 1. Introduction

The dynamic growth of transport generates an increasing demand for energy. Depletion of fossil fuels and the practical limitations of alternative propulsion systems, especially for applications in the heavy-duty, marine and off-road sectors, serve as incentives to scale up renewable alternative fuels [1]. In recent years researchers increased their efforts in the exploitation of various feedstock for biofuel production. This included amongst others rapeseed [2], camelinas [3], pongamia [4], cashew nut [5], ligno-cellulosic [6] or animal waste fats [7], [8]. However, estimates indicate that development of the current two commercially exploited bio-oil-based diesel substitutes, fatty acid methyl esters (FAME) and hydrotreated vegetable oil (HVO), will cover only half the increase in fuel demand by 2040 [9]. Therefore, immediate actions should be taken to diversify the feedstock for production of alternative fuels.

Investigation of the end-to-end efficiency and environmental impact of pyrolysis oils is currently high on the agenda of worldwide research [10], [11], [12]. Pyrolysis enables safe valorisation of various

materials for engine fuels, often taking advantage of their different chemical make-up [13]. Utilisation of end-of-life tyres poses a particular challenge, yet provides sufficient energy density to make their pyrolysis economically feasible [14].

On a molecular level, tyre pyrolysis oil (TPO) consists of valuable hydrocarbon fractions which cover a wide range of boiling points, including light naphtha (< 70 °C), heavy naphtha (71-182 °C), kerosene (182-260 °C), diesel (260-338 °C) and gasoil (338-566 °C) [15]. Depending on feedstock and processing technology, TPO's kinematic viscosity ranges from 1.7 to 17.8 cSt. Its density is from 871 to 995 kg/m3, and its calorific value ranges from 40 to 44 MJ/kg [16], [17]. Its molecular structure is characterised by a low hydrogen-to-carbon ratio, typically varying between 1:10 and 1:11 [18]. After distillation and pre-treatment, the physical properties of TPO are similar to diesel fuel (DF), but several characteristics prevent its direct use in a compression-ignition engine. Crude TPO´s sulphur content is the biggest hurdle [19]. It ranges from 500 ppm to 4000 ppm, depending on feedstock and pyrolysis conditions [14]. Additionally, TPO has a high content of heteroatomic molecules and a high concentration of aromatic compounds.

Production process parameters determine the physicochemical properties of crude TPO. For detail discussion on this topic the reader is referred to the review by Mikulski et. al. [20]. However, regardless of the technology, the sulphur content of the final fuel product exceeds normative limits. Catalysts are often used at the pyrolysis stage to reduce sulphur in liquid products. Aydin et al. [14] demonstrated that a 5% addition of calcium hydroxide $Ca(OH)_2$ or calcium oxide (CaO) reduced sulphur content from 1.4% to 0.9%, relative to the process without the addition of a catalyst. However, the researchers reported that this is the lower limit achievable.

The most commonly used desulphurisation methods for pyrolysis oil are hydrotreating, solvent extraction and fractionation [21]. Al-Lal et al. [22] made a comprehensive review of TPO refining technologies, highlighting boiling point shift by alkylation and desulphurisation by extraction, precipitation or adsorption. However, none of the mentioned treatment methods yielded a product directly applicable to automotive applications. Fractionation can be tailored to suit the expected application of the obtained fractions. Roy et al. [23] demonstrated the potential use of the light fraction

of pyrolysis oil as a gasoline substitute or gasoline additive; the medium fraction as a plasticiser in rubbers; and the heavy fraction as a DF equivalent.

On the end-user side, most knowledge regarding combustion and emissions of TPO comes from legacy (pre-Euro standard) engines operating in sub-optimal combustion conditions [20]. Tests on modern automotive engines are confined to small TPO admixtures, not exceeding 10%, and mostly performed using factory, diesel-optimised calibration maps. For instance, Martinez et al. [24] tested a diesel blend with 5% TPO in a 2-litre, four-cylinder, turbocharged car engine. In the low-load range, the TPO additive had a negative effect on both thermal efficiency and hydrocarbon emissions. Notably, the authors used Fourier transform infra-red (FTIR) multi-compound gas analyser and particulate matter (PM) size spectrometer. The detailed exhaust analyses showed that TPO admixture increased aromatics concentrations and shifted the PM size distribution towards larger number of smaller particles. The TPO additive also increased oxides of nitrogen ($NO_X$) emissions, regardless of load. An increase in combustion duration, relative to operation on DF, was also noted. Mikulski et al. [25] emphasised the role of distilled, light TPO fractions as viscosity improvers to enable the use of straight vegetable oil in Euro III mid-duty on-road engines with common-rail injection systems. For a ternary mixture of TPO, cold-pressed rapeseed oil and diesel (5%, 55%, and 40% by volume respectively), efficiency and emissions results were superior compared to FAME-based biodiesels.

Studies using TPO-DF blends in legacy stationary diesel engines have produced mixed results. Murugan et al. [26] tested blends in an engine with a low-pressure, direct, mechanical injection system, at 1500 rpm and up to 0.53 MPa in brake mean effective pressure (BMEP). They observed a monotonic increase in $NO_X$, unburnt hydrocarbons (HC) and carbon monoxide (CO) emissions as the TPO content in the mixture increased up to 70%. This was explained by the aromatics content, higher viscosity and lower volatility of TPO. The authors concluded that up to 20% TPO can be added to DF without a noticeable effect on efficiency or emissions, but higher admixtures require improvement of fuel quality. Testing with distilled TPO, the same authors [27] used 90% TPO fuel and found a 3% efficiency deterioration. Combustion of this mixture produced approximately 20% more smoke than when using DF, but reduced $NO_X$ emissions by a similar extent. Ilkiliç and Aydin [28] performed experiments with

a similar engine. They found that blends with up to 35% TPO can be used effectively without any engine modifications. Frigo et al. [29] carried out performance and emissions tests on a similar engine using TPO blends of 20% and 40% in DF. They reported that there was no significant difference in engine performance and emission values when using 20% TPO admixture, but there was a deterioration in engine combustion characteristics when TPO content was increased to 40%. In particular, they observed auto-ignition was delayed by approximately 5 crank angle degrees (CAD). Karagöz et al. [30] also used a simple stationary engine with mechanical fuel injection for testing mixtures of DF with TPO (10%, 30% and 50%) at a constant speed of 2000 rpm. Engine load varied from 0.11 to 0.43 MPa in BMEP. A decrease in thermal efficiency was noted as TPO concentration increased. The ignition delay was also observed. However, in contrast to other works, $NO_X$ emissions increased with rising TPO content, whereas smoke opacity, HC and CO emissions decreased. Chwist et al. [31] reported a decrease in CO and $NO_X$ emissions, while the changes in HC emissions were ambiguous in the range of up to 20% TPO admixture.

These discrepancies in results intuitively can be attributed to different fuel properties: TPO parameters strongly depend on feedstock type, pyrolysis conditions and fuel post-processing. However, none of the above-referred studies investigated TPO's sensitivity to the combustion regime. Instead, all the studies were performed at fixed, single fuel-injection timings, although timing was different for different studies. As a result, the combustion could be shifted to the premixed mode or mixing-controlled mode, depending on engine settings. This provides different emission trends for different fuel properties. Notably, most studies seem methodologically outdated in terms of current engine research. Contemporary diesel engines employ multiple-injection strategies and sophisticated air-path control, including boost, temperature conditioning and exhaust gas recirculation (EGR) to achieve partially-premixed compression ignition (PPCI) and to reduce emissions of both $NO_X$ and PM in tandem [32].

More recently, Mikulski et al. [33], the authors of the present work, proved that large-scale (up to 40%) TPO blends can perform well under the PPCI regime, preparatory to state-of-the-art combustion engines. Using split-injection strategies and cooled EGR, the authors proved US EPA Tier 4 emission limits compliance with TPO-based fuels without engine re-calibration. The work provided further

insight into differences in combustion characteristics in the premixed phase between DF and TPO surrogates. The study also focused on non-legislative emissions. Among different species, the production of sulphur oxides, aromatics and formic acid was found to increase with TPO.

Summarising the literature review, despite the abundant worldwide research into TPO combustion, insufficient attention has been paid to TPO fuel sensitivities to combustion conditions, especially when considering modern combustion systems. There is a lack of comprehensive proposals to co-optimise injection and air-path parameters to suit TPO properties, in search of optimal emissions and efficiency.

This paper presents research aimed at filling this knowledge gap. The work is based on the results of TPO characterisation at nominal engine conditions, presented by Mikulski et. al. [33], and extends the insight into combustion optimization with injection timing. This was preceded by a comprehensive analysis of the physicochemical properties of the fuels. This enables selecting a distilled TPO fraction that could be blended with DF up to 40%, while maintaining DF standards compatibility. A complex analysis of the fuel injection strategy under fully controlled thermal conditions was carried out for the first time in this work. The analysis involves over 64 original operating conditions unexplored earlier. The design of the experiments covers a combination of 2 injection parameters (energization of the pilot and main injection pulse) and EGR. This allowed establishing of engine controls satisfying optimal emissions for the tested fuels without deteriorating efficiency. The emissions target was compliance with EU Non-road Mobile Machinery (NRMM) Stage V limits. The work further provides unique insight into relevant non-legislated emissions at optimized conditions, that can influence uptake in the fuel market.

## 2. Test fuels

This study tested high admixtures of TPO in DF, namely 20% and 40% fractions on a mass basis, referred to as TPO20 and TPO40. The TPO originated from an industrial production process involving a rotary kiln reactor with a capacity of 8 tonnes. The feedstock was mixed car tyres provided directly to the reactor, without any pre-treatment. After condensation, the crude TPO was subjected to two-stage filtration, including in a Büchner funnel with a 0.13 mm mesh on the fine filter side. Table 1 shows the

most important properties of the crude TPO and the tested blends, with DF as a reference. Note that the DF was a pump-grade arctic fuel, which did not contain any bio components.

Table 1. Physical and chemical parameters of the fuels. Fuel characterisation data adopted from Mikulski et al. [33].

| Parameter | DF | TPO | TPO20 | TPO40 |
|---|---|---|---|---|
| Density @ 15°C [kg/m$^3$] | 826 | 948 | 844 | 867 |
| Viscosity @ 40 °C [mm$^2$/s] | 2.3 | 15.3 | 3.0 | 3.9 |
| Flashpoint [°C] | 61 | 90 | 61 | 61 |
| Sulphur content [mg/kg] | 6.1 | 5000 | 1154 | 2265 |
| Water content [mg/kg] | 11 | 410 | 86 | 141 |
| Higher heating value [MJ/kg] | 44.8 | 44.7 | 44.7 | 44.8 |
| Cetane index | 40.1 | 32.6 | 38.2 | 36.1 |

Although crude TPO's viscosity enables its drop-in use for engines, its low flashpoint implies safety issues. Therefore, we used a distilled heavier TPO fraction, obtained in the temperature range of 330-375 °C. The tested fuel blends have parameters meeting the applicable standards, except the sulphur content.

The fuel samples were subjected to physical and chemical analysis. This followed the respective standards for testing DF and alternatives. A comprehensive discussion of the fuel analytics methods, including their accuracy, is provided in previous work by the authors [33].

The detailed chemical composition of the tested fuels was identified by gas chromatography and mass spectrometry (GC-MS). DF was identified as composed mostly of hydrocarbons $C_{11}$-$C_{18}$, while TPO contained mainly hydrocarbon chains between $C_{17}$ and $C_{24}$, with an overall share of $C_{21}$ and higher topping 46.4% (Fig. 1). As for hydrocarbon type, TPO contained approximately 5% olefins, 55% alkanes and 40% aromatics. DF, on the other hand, contained approximately 27% aromatics, topped up by almost

solely saturated hydrocarbons - alkanes and cycloalkanes. The higher aromatic content of TPO is ultimately responsible for its lower cetane index, as shown in Tab. 1.

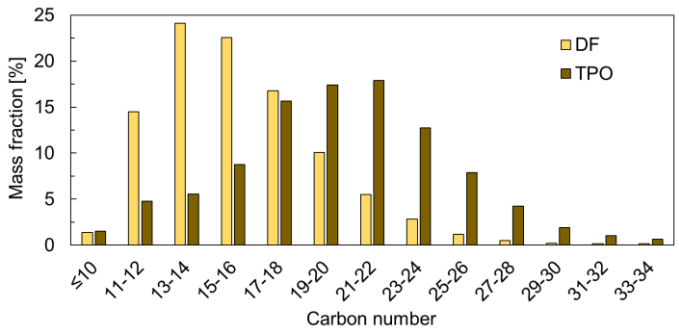


Figure 1. TPO and DF split into molecule carbon numbers. Reproduced from [33] with permission from Elsevier.

## 3. Research engine and procedures

### 3.1 Research engine

Engine experiments were performed at the Lublin University of Technology in Poland, with a state-of-the-art, four-stroke, light-duty, single-cylinder research engine. The AVL 5402 is a common-rail (CR) direct injection engine with a 510 $cm^3$ displacement and a 17:1 compression ratio. Table 2 lists the governing parameters of the tested engine.

The engine has a four-valve head with tangential and helical ports to control swirl. It has an in-piston toroidal combustion chamber. The high-pressure Bosch CP 4.1 fuel pump feeds a seven-hole electromagnetic injector with a 145° included spray angle. Injection parameters are controlled by a fully open Bosch engine controller, managed via ETAS INCA software. The fuel line is thermally conditioned by an AVL 753C temperature conditioner and consumption measured by an AVL 733S dynamic fuel meter.

Figure 2 illustrates the test stand setup. The air path includes an electrically-driven Roots compressor (Eaton M45) capable of providing up to 2 bar boost pressure. The high-pressure EGR loop and exhaust runner are equipped with proportional electro-valves for accurate EGR rate control and to mimic turbine backpressure. Both engine and the compressor have in-house thermal conditioning systems to maintain

coolant, lubricant, charge air and EGR circuit at required constant temperatures, to within +/- 0.5 °C accuracy. The engine is coupled to an asynchronous motor dynamometer with speed control from AVL to apply load and stabilise rotational speed.

Table 2. Research engine specifications

| | |
|---|---|
| Type | AVL 5402 |
| Configuration | four-stroke, single-cylinder |
| Bore / Stroke | 85 / 90 mm |
| Displacement | 510.5 cm3 |
| Compression ratio | 17:1 |
| Swirl ratio | 1.7:1 |
| Combustion chamber | Mexican hat |
| Injection system | CR, Bosch CP4.1; 180 MPa; multi-pulse capability |
| Intake path | Electrically-driven Eaton M45 compressor; with thermal management |
| EGR system | high-pressure, with thermal management |
| Engine management | AVL-RPEMS, ETK7-Bosch |
| IVO / IVC | 712 / 226 CAD |
| EVO / EVC | 488 / 018 CAD |

*) IVO/EVO/IVC/EVC – intake/exhaust valve opening/closing

(a)

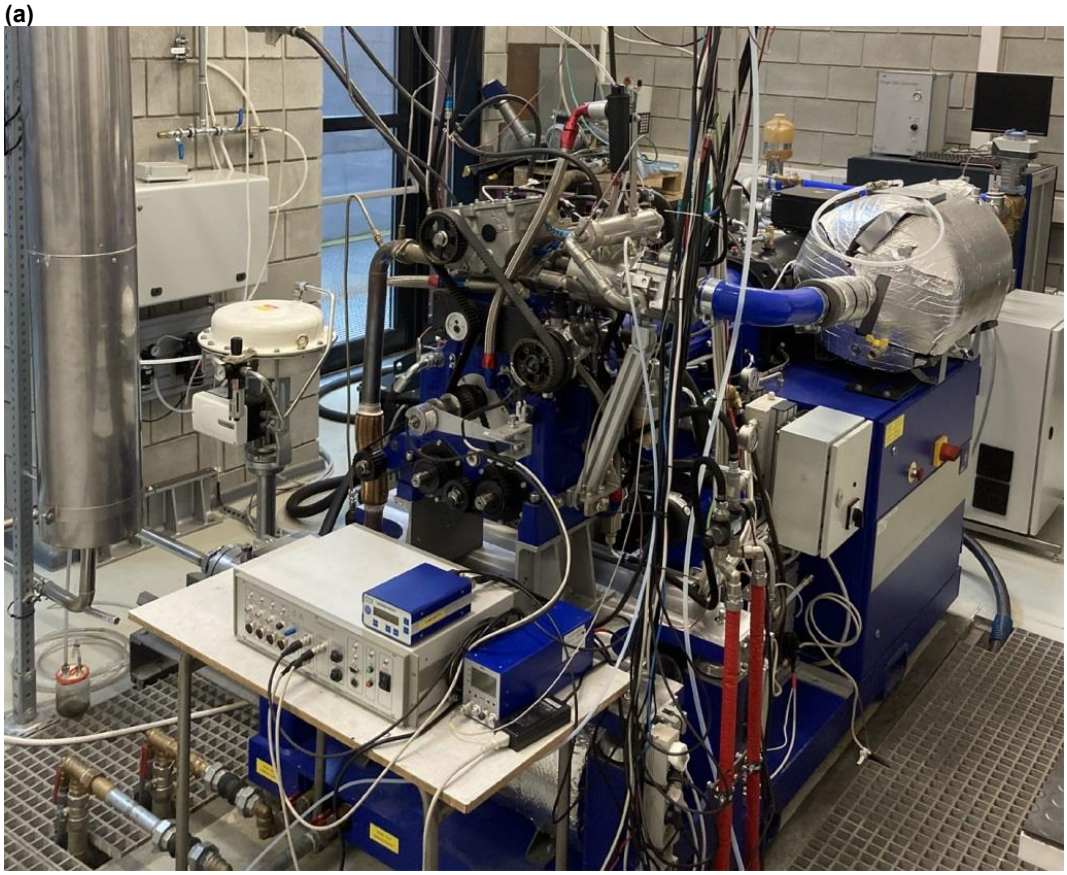

(b)

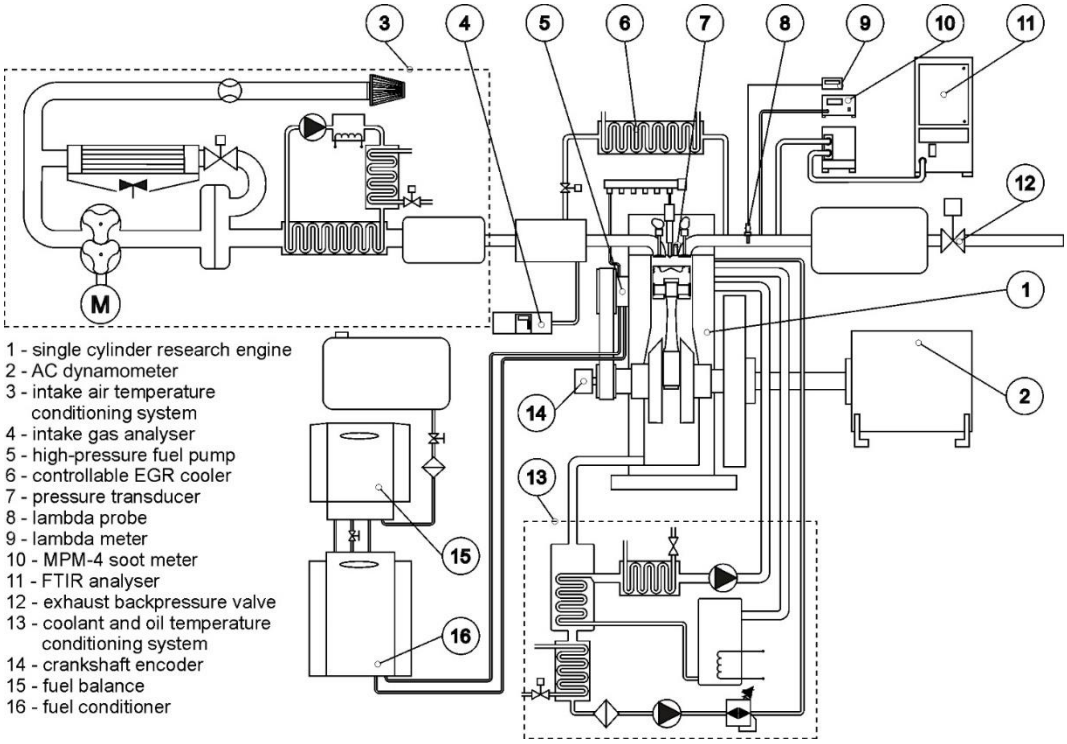


Figure 2. Photography (a) and diagram (b) of the engine test stand

Table 3. Engine test bench measurement equipment and accuracy. Equipment accuracy data adopted from [33].

| Measurand | Transducer | Range | Accuracy |
|---|---|---|---|
| In-cylinder pressure | AVL GU22C | 0-25 MPa | 0.25-1.0%[1)] |
| Fuel consumption | AVL Fuel Mass Flow Meter 733S | 0-125 kg/h | 0.12% |
| Excess air ratio ($\lambda$) | Bosch LSU 4.2 / ETAS LA4 | 0.7-2.8 | 1.5% |
| Air mass flow rate | E+E Elektronik EE741 | 2.6-1000 kg/h | 3% |
| Intake/exhaust pressure | WIKA A-10 | 0-4 bar | 0.5% |
| Temperature (ambient, intake air, EGR, cooling, oil, fuel) | Pt100 Czaki TP-361 | -40-400 °C | 0.2% |
| Exhaust temperature | Thermocouple K Czaki TP-204 | 0-1200 °C | 0.8% |
| Exhaust CO | AVL Sesam FTIR | 1-10000 ppm | 0.36% |
| Exhaust HC | AVL Sesam FTIR | 1-1000 ppm[2)] | 0.1-0.49%[3)] |
| Exhaust $NO_X$ | AVL Sesam FTIR | 1-4000 ppm | 0.31% |
| Exhaust PM concentration | Maha MPM4 | 0-700 mg/m$^3$ | 0.1 mg/m$^3$ |
| Intake $CO_2$ | Hermann-Pierburg HGA 400 | 0-20 % | 0.1% |

[1)] Depending on temperature.

[2)] Given measurement span relates to the concentration of a single identified hydrocarbon.

[3)] Depending on the type of hydrocarbon species.

The EGR rate was calculated from the $CO_2$ ratio between the intake and the exhaust gas. The concentration of $CO_2$ on the intake side was measured via a Hermann-Pierburg HGA 400 gas analyser. The excess air ratio was measured using a Bosch LSU 4.2 lambda probe and ETAS LA4 lambda meter, considering back-pressure compensation [34]. The concentrations of 23 regulated and non-regulated exhaust gas components were recorded by an AVL FTIR multi-component analytical system. A Maha

MPM-4 analyser measured particulate concentration. Table 3 lists the key measuring devices with their accuracy.

An AVL GU22C piezoelectric pressure transducer is installed directly in the engine head for combustion analysis. Recording of the pressure signal is triggered using an optical encoder, with a constant angular resolution of 0.1 CAD. The signal was recorded for 100 consecutive engine cycles at each operating point. The obtained values were cycle-averaged and pegged using intake and exhaust pressures to provide absolute pressure.

Thermal parameters and low-frequency signals were acquired via a test stand automation system, based on a programmable logic controller and in-house software. All the parameters, together with exhaust analyser data, were recorded every single second and averaged for 30 seconds.

### 3.2. Research matrix

The engine research was divided into two stages. The first stage covered the five operating points under the ISO 8178 type D2 protocol for stationary engines. This represents a load sweep at a constant engine speed (1500 rpm), as outlined in Tab. 4. The baseline engine calibration during this test phase involved a split fuel-injection with a constant dwell between the two fuel doses. Start of injection (SOI) timings were varied, providing the start of the main heat release near top dead centre (TDC) for reference DF. The mass of the pilot fuel injection was varied accordingly, as shown in Tab. 4. Boost pressure was increased with load to provide sufficient air excess at given fuel values.

The second stage of the research was performed at a single operating point, at IMEP of 0.5 MPa. This corresponds to a point in the test making a large contribution to the overall test emissions. Fuel injection timings and the EGR ratio were swept in order to investigate engine response to variable control parameters when fuelling with TPO. The manifold absolute pressure (MAP), along with other parameters, were kept at reference set points outlined in Tab. 4. Tests were performed under stable thermal conditions. The engine coolant, lubricating oil and recirculated exhaust gas at the manifold inlet were set at 85 °C. The temperature of the intake air was kept fixed at 35 °C. The final aspirated charge temperature resulted from the enthalpy balance between fresh air and EGR, and was left uncontrolled,

as during normal engine operation. The fuel temperature at the inlet to the high-pressure pump was set at 30 °C.

Table 4. Engine operating conditions and control parameters

| Load [%] | 10 | 25 | 50 | 75 | 100 |
|---|---|---|---|---|---|
| IMEP [MPa] | 0.2 | 0.5 | 0.8 | 1.1 | 1.4 |
| MAP [kPa] | 100 | 125 | 140 | 155 | 175 |
| λ [-] | 5.2 | 2.8 | 2.0 | 1.7 | 1.55 |
| SOI1 [CAD] | 342 | 342 | 340 | 340 | 340 |
| SOI2 [CAD] | 356 | 356 | 354 | 354 | 354 |
| Fuel pressure [MPa] | 50 | 60 | 70 | 80 | 80 |
| Pilot fuel quantity [mg] | 1.5 | 1.6 | 1.7 | 1.7 | 1.7 |
| Pilot fuel fraction [%] | 20 | 11 | 7 | 5 | 3.7 |

### 3.3. Data analysis procedures

Combustion analysis, based on in-cylinder pressure, was carried out using AVL Boost software. The calculations took into account gas-flow models, internal EGR estimation and heat transfer through the cylinder walls, estimated by the Hohenberg correlation [35]. The heat release rate (HRR) was obtained by subjecting the cylinder pressure to a first-law analysis, using the following formula:

$$\mathrm{HRR} = \frac{\gamma}{\gamma-1} p \cdot \Delta V + \frac{1}{\gamma-1} V \cdot \Delta p - \Delta Q_{\mathrm{ht}}, \quad (1)$$

The HRR values presented in the paper are gross values, taking into account the calculated heat transfer ($Q_{\mathrm{ht}}$) rate. The cumulative HRR values were used as the basis for calculating the mass fraction burned (MFB), which in turn allowed calculation of combustion timing indicators.

The molar concentrations of exhaust gas components, measured directly using "wet" effluent gases, were converted to specific emissions, taking into account atomic fuel composition, excess air ratio and

specific fuel consumption. The PM emission was measured on a mass-per-volume basis and then converted to indicated specific values.

In order to provide repeatability, the tests at each operating point were conducted three times and in a different sequence, after changing the fuels and flushing the system. The maximum measurement error for directly measured values was then taken as either the standard deviation from these three samples or as device accuracy, depending on which value was higher. The measurement error for indirectly calculated values was derived according to the method of partial derivatives by Kline and McClintock [36]. A detailed discussion of uncertainty analysis for this engine setup, together with more information on the measurement devices used in this study, is to be found in Mikulski et al. [33].

# 4. RESULTS AND DISCUSSION

## 4.1. Analysis of combustion

The complete combustion analysis for the test fuels at nominal conditions (Tab. 4) was established by Mikulski et al. [33]. Thus, a comprehensive discussion is omitted here, and only pressure traces for subsequent operating points with DF reference are shown in Fig. 3. This aims to provide context for discussing the effects of control parameters on combustion. It is evident from Fig. 3 that the intensive pressure rise rate commences at top dead centre (TDC) for each condition. The overall combustion duration is elongated with increasing load, resulting in retarded combustion centre (CA50). This strategy aims to keep $NO_X$ within the emission limit while maintaining the indicated thermal efficiency above the 40% target for engine calibration with DF. Note that these targets were met for nominal calibration (Tab. 4) without external EGR.

Without EGR, fuel-to-fuel differences in combustion manifest only at low-load conditions [33], substantiating the focus of the fuel-individual optimisation endeavour on the 0.5 MPa IMEP point. Figure 4 plots the HRR values for this operating point when fuelling with DF and TPO40, also showing combustion response to external EGR.

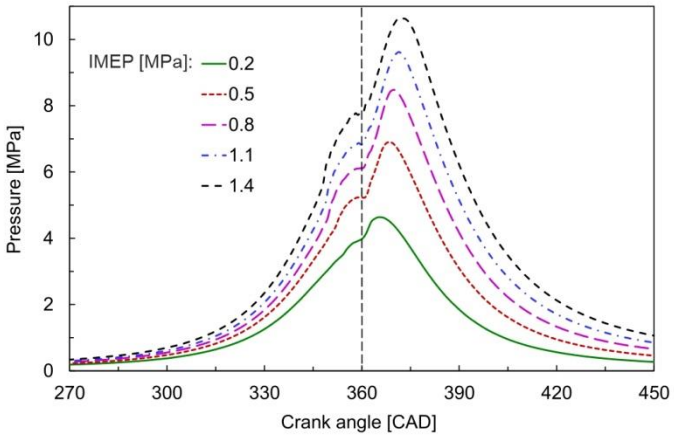


Figure 3. In-cylinder pressure at variable loads for DF at reference conditions, shown in Tab. 4

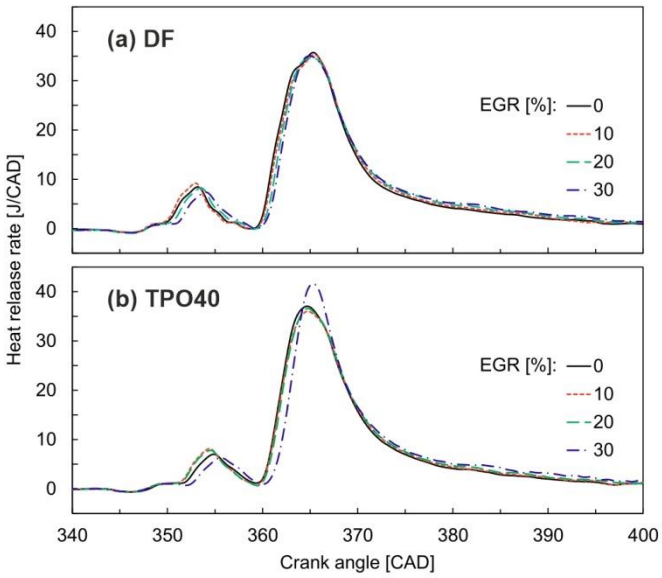


Figure 4. EGR effects on HRR for DF and TPO40; 0.5 MPa IMEP, reference SOI

It is apparent from Fig. 4 that, despite the same SOI, the pilot fuel ignition is substantially delayed for TPO40 compared with DF. This delay, of approximately 2 CAD, originates from a substantially lower cetane index and lower volatility, influencing both the physical and chemical ignition delay of TPO. Another characteristic fuel-to-fuel difference is that the pilot fuel combustion is less complete for TPO samples. The fuel-to-fuel differences diminish in the main combustion phase and any that remain can be attributed to the pilot fuel function. For less-reactive TPO40, delayed and less complete combustion of pilot fuel provides more reactive species at the moment of main fuel injection. They advance combustion chemically and compensate for TPO´s lower cetane number, so the start of

combustion is controlled diffusively. Furthermore, the lower cumulative heat release during pilot fuel combustion results in more energy provided during the main combustion phase. This is apparent in the higher peak HRR values for TPO40 observed in Fig. 4 b.

According to the same reasoning, the addition of EGR primarily affects the premixed pilot combustion phase. The effects are substantial but non-monotonic. For example, according to Fig. 4b, mid-range EGR additions (up to 20%) can stimulate pilot fuel HRR, while heavy EGR can suppress it considerably, affecting the main HRR in the later phase. The non-monotonic effect of EGR originates from the superposition of thermal and chemical effects. On the thermal side, the start of compression temperatures increase due to higher recirculated gas temperature than intake air [37]. However, the lower specific heat of the EGR mixture reduces end of compression temperature, when compared to the air compression. On the chemical side, the recirculated gas contains CO, NO, unburned hydrocarbons and reactive, partially reformed species, which affect preliminary, low-temperature reactions [38]. Irrespective of these conflicting effects, it is evident in Fig. 4 that EGR elongates the afterburning period (starting from 370 CAD) to a similar extent for both fuels.

This complexity of the PPCI concept, illustrated here by the EGR response, makes knowledge-based calibration for different fuels a challenging endeavour. Emission characteristics of those fuels at nominal conditions can provide additional knowledge supporting the choice of calibration parameters. This is discussed in the following subsection.

### 4.2. Fuel-to-fuel differences in emissions at standard calibration

The previous subsection´s analysis of combustion provides context for understanding the emission results. These are depicted in Fig. 5 on the indicated specific basis for standard calibration, without EGR. As already mentioned, at high loads there are no significant differences in HRR between the tested fuels. Thus, any differences in emissions that manifest in load points from 0.8 MPa to 1.4 MPa IMEP stem from differences in the fuels´ properties and their chemical make-up.

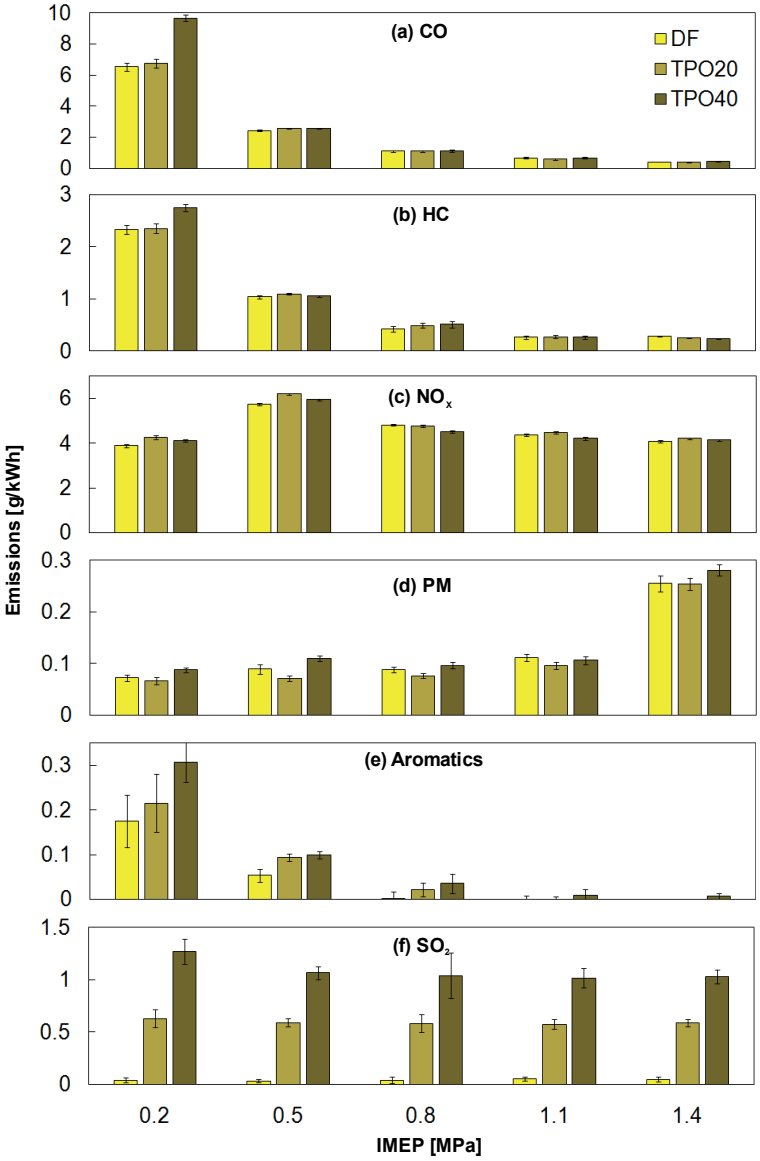


Figure 5. Indicated specific emissions of regulated and non-regulated exhaust compounds at reference conditions

It is evident from Fig. 5 that in the high-load regime, without significant changes to the combustion characteristics, TPO admixtures do not affect CO, HC or $NO_X$ emissions. All are comparable to DF within the limits of statistical relevance. Thus, these quantities are not influenced by fuel composition and remain sensitive only to engine control parameters. Elevated PM emissions, along with high aromatics and $SO_2$ concentrations, observable across all operating points in Fig. 5, primarily are attributed to TPO's chemical make-up. Section 3 gives the data on the fuels´ sulphur and aromatic contents. PM formation is supported by fuel contaminants - particularly sulphur [39] - yet remains highly sensitive to the mixture conditions during combustion [40].

Focusing on the 0.5 MPa IMEP point, foreseen for recalibration, Fig. 5 implies that CO and $NO_X$ emissions are elevated by 6% and 7% respectively when using TPO20 instead of DF. Those differences shrink to about 2% when fuelling with TPO40. However, PM emissions for TPO40 are significantly higher (by about 22%) compared to DF. For TPO20, PM emissions are less than with DF by the same order of magnitude. Hence, combustion of TPO20 and TPO40 exhibit the opposite sides of the $NO_X$/PM trade-off.

Finally from Fig. 5, note that the 0.5 MPa operating point has the highest overall $NO_X$ emissions across the engine operating envelope. Crucially, it also has the highest weight in the ISO 8178 D2 test cycle.

### 4.3. Emission control strategy for TPO

The above paragraph suggests that $NO_X$ and PM can be significantly influenced by the fuel's effect on combustion. This is a well-known trade-off for compression ignition engines [41], [42]. External EGR is typically used when aiming for a low-$NO_X$ calibration. Simultaneously, the effect of EGR on combustion phasing, and hence, efficiency and emissions, can be mitigated by adjusting injection timing [43]. The combustion concept discussed here uses two sequential injections to realise the PPCI principle. The ratio and dwell between the pilot and main injection are carefully adjusted to provide superior emission and performance characteristics. This optimum calibration window is usually very narrow, and any attempts to modify either the dwell or fuel-split ratio usually lead to drastic deterioration of the characteristics. Due to this close-bound relation of pilot and main injections, robust incremental improvement of engine performance under changing fuel quality is usually achieved by shifting the start of both pilot (SOIp) and main injection (SOIm) by a common factor of SOI shift. In other words, PPCI using EGR and SOI as calibration parameters, allows decoupling the optimisation of emissions and efficiency, thus managing the system complexity issue. This emission control strategy is followed in this work for TPO, aiming for a favourable $NO_X$/PM trade-off for different fuel blends, without jeopardising other emissions. The results for $NO_X$ and PM are graphically presented in Fig. 6 and Fig.

7. Both figures show absolute values for DF reference fuel, whereas for TPO blends the figures give the emission differences between the given fuel and DF.

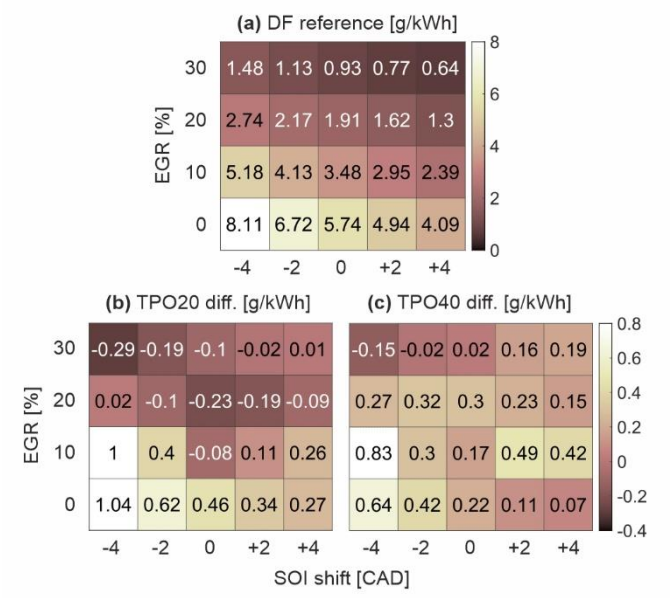


Figure 6. Indicated specific emissions of $NO_X$ for DF and differences in emissions for TPO20 and TPO40 at variable SOI and EGR rates

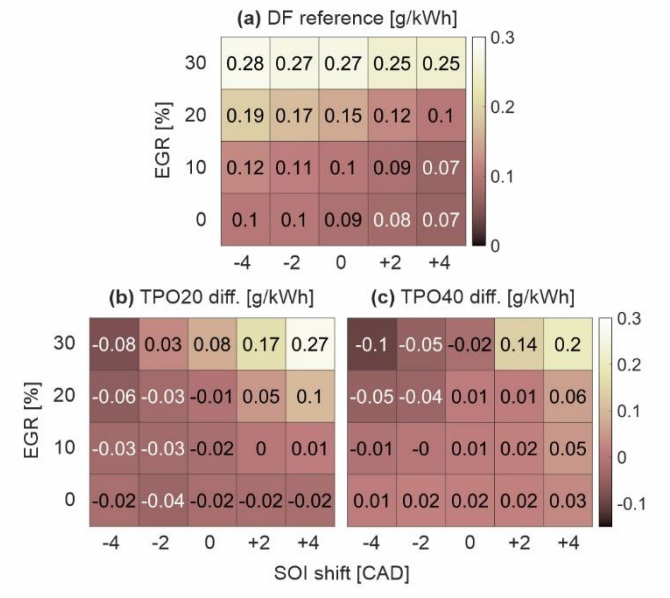


Figure 7. Indicated specific emissions of PM for DF and differences in emissions for TPO20 and TPO40 at variable SOI and EGR rates

The EGR trade-off between $NO_X$ and PM is evident when comparing the results for DF reference fuel in Fig. 6a and Fig. 7a (the top matrix in both figures). The lowest $NO_X$ emissions are achieved for high EGR rates (the top row of Fig. 6a), whereas the lowest PM values are found on the opposite side of the calibration map (the bottom row of Fig. 7a).

Importantly, when using higher EGR rates and advanced SOI, both $NO_X$ and PM emissions from TPO20 and TPO40 admixtures are lower than the DF baseline. This more-premixed combustion regime is favourable for TPO due to its lower volatility (refer to flash point values of TPO vs DF in Tab. 1). On this top-left corner of the calibration map (SOI advanced by 4 CAD and 30% EGR) TPO20 can achieve superior $NO_X$ emission results at the same calibration, at an indicated specific level of 1.19 g/kWh vs. 1.48 g/kWh for DF. In comparison with the nominal non-EGR DF calibration, these values equate to an 80% reduction for TPO20 vs. a 75% reduction for DF. At the same time, this low-$NO_X$ calibration is accompanied by PM emissions that are doubled for TPO20 and tripled for DF. The corresponding results from this same low-$NO_X$ calibration for TPO40 are similar to that of TPO20, although the $NO_X$ improvement is slightly less pronounced and the PM penalty is lower. The top-right corner of the calibration map also deserves comment. Here, with late SOI and 30% EGR, the PM emissions from both TPO admixtures are double those of DF, revealing TPO´s sensitivity to SOI at high EGR rates. In contrast, the level of PM emissions from DF was unaffected throughout the investigated SOI sweep at heavy EGR.

Figures 8 and 9 supplement the above discussion on the calibration parameters by depicting the HC and CO emissions across the same matrices. It is evident from Fig. 8 that HC is generally reduced with increased EGR, as more of the unburned hydrocarbons are recirculated back to the cylinder and oxidised during the next cycle. This mechanism dominates the reduced HRR during the afterburning phase associated with EGR dilution which leads to diffusion flame quenching (refer to Fig. 4 and associated discussion).

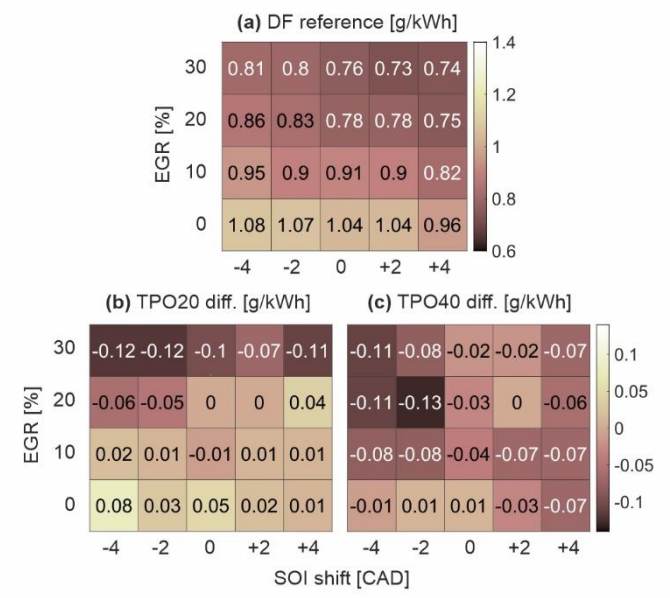


Figure 8. Indicated specific emissions of HC for DF and differences in emissions for TPO20 and TPO40 at variable SOI and EGR rates

Abstracting from the phenomenology, however, both DF and TPO fuels exhibit improved HC emissions in the high-EGR regime. TPO fuels ultimately exhibit slightly better potential for HC reduction at low-$NO_X$ calibration than DF. The emission of CO, depicted in Fig. 9, does not show large sensitivity to calibration parameters. CO can be minimised for DF in a regime of mild EGR regime and late injections. TPO does exhibit noticeably worsen CO emissions than DF, except in high-EGR conditions, where CO is more than 25% higher. At the same calibration point that brings the greatest low-$NO_X$ benefits for TPO, the CO emission was higher than with DF by 22% and 12% for TPO20 and TPO40 respectively. However, reducing the EGR rate to 20% and using early injections keeps some benefits of simultaneous $NO_X$, PM and HC reductions without any CO penalty.

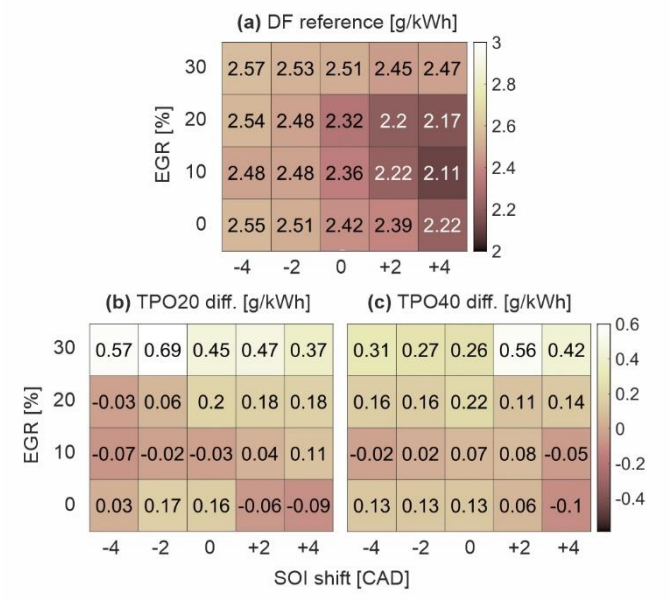


Figure 9. Indicated specific emissions of CO for DF and differences in emissions for TPO20 and TPO40 at variable SOI and EGR rates

Other, non-legislative emission components that pose a challenge for TPO (Fig. 5) are excluded from the calibration parameter sensitivity study. As discussed earlier, elevated emissions of aromatics and $SO_2$ are attributed to TPO´s respective aromatic and sulphur contents, and, as such, cannot be directly controlled by optimising combustion. Note, however, that aromatic hydrocarbons correlate with total HC emissions (Fig. 5). $SO_2$ emission, on the indicated basis, shows only slight variations across the calibration space as the indicated efficiency changes slightly. However, the effect is below the statistical relevance of the combined emission and fuel consumption measurement accuracy.

### 4.5. Summary of emissions and thermal efficiency

To provide an overall picture of fuels' response to control parameters, an emission indicator (E) was calculated using the following formula:

$$E = \frac{CO}{CO_{min}} + \frac{HC}{HC_{min}} + \frac{NOx}{NOx_{min}} + \frac{PM}{PM_{min}} - 4 \quad (2)$$

The symbols of chemical compounds represent indicated emissions, whereas the minimum values (denominators) are determined for DF and can be read from Figs. 6a-9a. The emission indicator is zero

if all components of Eq. 2 are at the minimum level achievable for DF. It is significant that the minimum emission points for different fuels do not coincide on the EGR/SOI maps. For DF, the minimum E value of 1.7 appears at 20% EGR and SOI retarded by 4 CAD (Fig. 10).

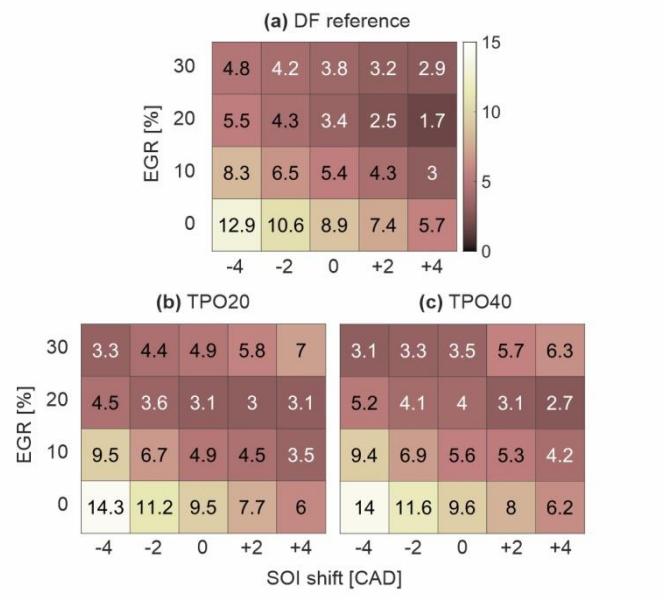


Figure 10. Over-limit values for DF, TPO20 and TPO40 at variable SOI and EGR rates

$NO_X$ and PM are the major factors influencing the emission indicator values shown in Fig. 10. For DF, the emission indicator map is almost solely shaped by $NO_X$, as this changes in the largest span. However, fuel-to-fuel differences are mostly influenced by PM emissions. Generally, TPO´s higher emission indicator values stem from its chemical propensity to create soot. This is particularly evident at the top right corner of the calibration maps, portraying late injection under heavy EGR conditions, which delays auto-ignition and prolongs combustion.

Figure 11 complements the picture with the results of indicated thermal efficiency (ITE), presented in the same form as in the case of emissions. While analysing the efficiency results one should note that the direct uncertainties in fuel consumption IMEP and engine-speed measurement mean the maximum error for indicated efficiency at the given operating point is +/-2 percentage points. Taking this into account, the differences in efficiency within the calibration envelope are majorly statistically irrelevant, both for DF and TPO blends. Referring back to Fig. 4, it is apparent that combustion onset remains

hardly sensitive to EGR. The main injection (SOIm) acts as a trigger for the main part of the heat release and determines how the energy is transferred to the piston work. This explains small efficiency differences obtained across the EGR lines in Fig.11. Note that the results in Fig. 4 correspond to the middle columns in Fig. 11a and 11c respectively.

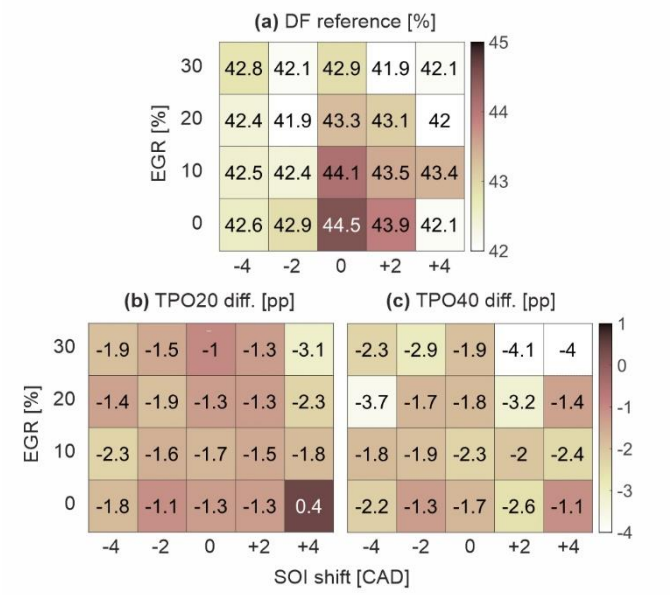


Figure 11. Indicated thermal efficiency for DF and differences in ITE for TPO20 and TPO40 at variable SOI and EGR rates

Nevertheless, despite statistical uncertainty, the results for DF indicate qualitatively that ITE appears reduced by both delay and advance of SOI from the reference point, as well as EGR increase. On average, ITE deteriorates by 2 percentage points as a consequence of any parameter shift from the reference point (zero SOI shift, non-EGR) to the boundary of the examined calibration space.

The differences in efficiency between the fuels across the calibration map in Fig. 11 are also noticeable. On average, the combustion of TPO20 instead of DF reduces ITE by 1.5 percentage points; for TPO40 the reduction is 2.3 percentage points. However, this may be attributable to the systematic error in the designation of the LHV of TPO and DF, set out in Tab 1. Note that the LHV measurements for DF and pyrolytic oils are performed according to different standards, and the errors for both methods are difficult to estimate. Thus, the fuel-to-fuel differences in indicated efficiency are to be treated as

ambiguous. The main takeaway from Fig. 11 is that the efficiency differences within the calibration map are too small to be statistically relevant.

Summarising the results of this section, the above conclusion concerning efficiency allows one to narrow down the calibration challenge (within the investigated area) to consider emissions only. Reverting to the discussion of Fig. 10, the best results, i.e., the minimum over-limit values, for both DF and TPO blends are obtained with mild (20%) EGR and SOI retarded by 2 CAD. Considering that $NO_X$ and PM are the main contributors to the overall emission maps, one can note that DF prefers delayed injection and mild EGR. In contrast, for TPO admixtures, comparable emission indicators can be achieved across a wider area of the control map. In particular, TPO outperforms DF at early injection and heavy EGR because TPO´s lower cetane index and poor volatility are enablers of PPCI combustion mode.

## 5. CONCLUSION

This study reports the results of the first comprehensive endeavour to optimise calibration of a modern, common-rail diesel engine to suit TPO fuels, aiming to establish an unbiased emission toxicity report for such fuels. It draws the following conclusions:

1. Contemporary engines employing a low-$NO_X$, partially premixed compression ignition mode can operate on TPO-based fuels without re-calibration. For the 40% TPO-diesel blend, combustion is affected only at low engine-loads, particularly with heavy EGR: start of combustion is delayed by up to 3 CAD. This increases hydrocarbon and CO emissions by 26% and 84% respectively. Elevated PM emissions at reference conditions result from TPO's chemical propensity to create soot.
2. In comparison with diesel, TPO can realise low-temperature, partially premixed combustion in a wider area of the calibration map. The favourable $NO_X$/PM mode is extended towards high EGR and early injection regimes, as the longer ignition delay of TPO supports creation of a premixed charge before auto-ignition.
3. Adopting this regime, contemporary engine control with dedicated calibration maps for TPO allows best-point $NO_X$/PM emissions of 1.22 g/kWh and 0.18 g/kWh respectively, while maintaining the

baseline indicated efficiency target of 42%. The corresponding best diesel calibration for both species yields 1.3 g/kWh and 0.1 g/kWh for $NO_X$ and PM respectively.

4. The cumulative legislated emission factor is still 36% higher for a calibration optimised for TPO than for diesel, due to elevated CO and HC emissions. These differences, however, remain insignificant in light of the current EU Stage V emission limits for stationary engines.

Conclusions 2-4 encourage us to re-think the axiom established by earlier studies that have categorised TPO fuels as "dirty." This study proves that opinions shaping this axiom are at least partially biased by the shortcomings of legacy engine technology. Unlegislated emissions remain the true concern for TPO. Regardless of calibration, TPO fuels emit more sulphur oxides. This correlates directly with fuel sulphur content, and as such cannot be mitigated by engine measures. Consequently, progress in inexpensive desulphurisation techniques could make TPO an affordable, carbon-neutral, alternative fuel for the off-road sector.

## ACKNOWLEDGEMENTS

The authors wish to thank AVL List GmbH for making the simulation software available within the AVL University Partnership Program framework.

The engine research was funded by the Lublin University of Technology statutory research, contract No. FD-20/IM-5/44.

## REFERENCES

[1] R. D. Reitz *et al.*, The future of the internal combustion engine:, *Int. J. Engine Res.*, vol. 21, no. 1, pp. 3–10, 2019,

[2] G. Koszałka, J. Hunicz, and A. Niewczas, A comparison of performance and emissions of an engine fuelled with diesel and biodiesel, *SAE Int. J. Fuels Lubr.*, vol. 3, no. 2, pp. 77–84, 2010,

[3] K. Duda, S. Wierzbicki, M. Śmieja, and M. Mikulski, Comparison of performance and emissions of a CRDI diesel engine fuelled with biodiesel of different origin, *Fuel*, vol. 212, pp. 202–222, 2018,

[4] S. Prakash, J. B. Sajin, and J. Ravikumar, Emission impact of pentanol on Pongamia biodiesel propelled diesel engine, *Int. J. Ambient Energy*, vol. 43, no. 1, pp. 237–242, 2019,

[5] Y. Devarajan, J. Ravikumar, D. Ragupathy, and H. Venu, Emissions analysis on second generation biodiesel, *Front. Environ. Sci. Eng.*, vol. 11, no. 1, pp. 1–6, 2017,

[6] S. Boopathi, J. Ravikumar, R. Devanathan, and S. A. A. Anicia, Injection and Exhaust Gas Recirculation Strategies for Reducing Emissions of Cyclohexanol-Diesel Blends in CI Engine, *Springer Proc. Mater.*, vol. 7, pp. 279–284, 2021,

[7] E. Thambiran, S. M. Rangaswamy, and J. Ravikumar, An experimental study on biodiesel production and impact of EGR in a CRDI diesel engine propelled with leather industry waste fat biodiesel, *Fuel*, vol. 321, p. 123995, 2022,

[8] M. Mikulski, K. Duda, and S. Wierzbicki, Performance and emissions of a CRDI diesel engine fuelled with swine lard methyl esters-diesel mixture, *Fuel*, vol. 164, pp. 206–219, 2016,

[9] Energy Outlook 2020 edition. https://www.bp.com/content/dam/bp/business-sites/en/global/corporate/pdfs/energy-economics/energy-outlook/bp-energy-outlook-2020.pdf (accessed Jan. 06, 2022).

[10] A. Quek and R. Balasubramanian, Liquefaction of waste tires by pyrolysis for oil and chemicals—A review, *J. Anal. Appl. Pyrolysis*, vol. 101, pp. 1–16, 2013,

[11] O. Azeta, A. O. Ayeni, O. Agboola, and F. B. Elehinafe, A review on the sustainable energy generation from the pyrolysis of coconut biomass, *Sci. African*, vol. 13, p. e00909, 2021,

[12] M. B. Figueirêdo, I. Hita, P. J. Deuss, R. H. Venderbosch, and H. J. Heeres, Pyrolytic lignin: a promising biorefinery feedstock for the production of fuels and valuable chemicals, *Green Chem.*, vol. 24, no. 12, pp. 4680–4702, 2022,

[13] H. Yaqoob, Y. H. Teoh, M. A. Jamil, and M. Gulzar, Potential of tire pyrolysis oil as an alternate fuel for diesel engines: A review, *J. Energy Inst.*, vol. 96, pp. 205–221, 2021,

[14] H. Aydin and C. Ilkiliç, Optimization of fuel production from waste vehicle tires by pyrolysis and resembling to diesel fuel by various desulfurization methods, *Fuel*, vol. 102, pp. 605–612, 2012,

[15] F. Campuzano *et al.*, On the distillation of waste tire pyrolysis oil: A structural characterization of the derived fractions, *Fuel*, vol. 290, p. 120041, 2021,

[16] W. Kaminsky and C. Mennerich, Pyrolysis of synthetic tire rubber in a fluidised-bed reactor to yield 1,3-butadiene, styrene and carbon black, *J. Anal. Appl. Pyrolysis*, vol. 58–59, pp. 803–811, 2001,

[17] M. M. Barbooti, T. J. Mohamed, A. A. Hussain, and F. O. Abas, Optimization of pyrolysis conditions of scrap tires under inert gas atmosphere, *J. Anal. Appl. Pyrolysis*, vol. 72, no. 1, pp. 165–170, 2004,

[18] J. D. Martínez, M. Lapuerta, R. García-Contreras, R. Murillo, and T. García, Fuel properties of tire pyrolysis liquid and its blends with diesel fuel, *Energy and Fuels*, vol. 27, no. 6, pp. 3296–3305, 2013,

[19] S. Murugan, M. C. Ramaswamy, and G. Nagarajan, A comparative study on the performance, emission and combustion studies of a DI diesel engine using distilled tyre pyrolysis oil–diesel blends, *Fuel*, vol. 87, no. 10–11, pp. 2111–2121, 2008,

[20] M. Mikulski, M. Ambrosewicz-Walacik, J. Hunicz, and S. Nitkiewicz, Combustion engine applications of waste tyre pyrolytic oil, *Prog. Energy Combust. Sci.*, vol. 85, p. 100915, 2021,

[21] J. S. Kim, Production, separation and applications of phenolic-rich bio-oil – A review, *Bioresour. Technol.*, vol. 178, pp. 90–98, 2015,

[22] A. M. Al-Lal, D. Bolonio, A. Llamas, M. Lapuerta, and L. Canoira, Desulfurization of pyrolysis fuels obtained from waste: Lube oils, tires and plastics, *Fuel*, vol. 150, pp. 208–216, 2015,

[23] C. Roy, A. Chaala, and H. Darmstadt, Vacuum pyrolysis of used tires end-uses for oil and carbon black products, *J. Anal. Appl. Pyrolysis*, vol. 51, no. 1, pp. 201–221, 1999,

[24] J. D. Martínez, J. Rodríguez-Fernández, J. Sánchez-Valdepeñas, R. Murillo, and T. García, Performance and emissions of an automotive diesel engine using a tire pyrolysis liquid blend, *Fuel*, vol. 115, pp. 490–499, 2014,

[25] M. Mikulski, M. Ambrosewicz-Walacik, K. Duda, and J. Hunicz, Performance and emission characterization of a common-rail compression-ignition engine fuelled with ternary mixtures of

rapeseed oil, pyrolytic oil and diesel, *Renew. Energy*, vol. 148, pp. 739–755, 2020,

[26] S. Murugan, M. C. Ramaswamy, and G. Nagarajan, Assessment of pyrolysis oil as an energy source for diesel engines, *Fuel Process. Technol.*, vol. 90, no. 1, pp. 67–74, 2009,

[27] S. Murugan, M. C. Ramaswamy, and G. Nagarajan, Performance, emission and combustion studies of a DI diesel engine using Distilled Tyre pyrolysis oil-diesel blends, *Fuel Process. Technol.*, vol. 89, no. 2, pp. 152–159, 2008,

[28] C. Ilkiliç and H. Aydin, Fuel production from waste vehicle tires by catalytic pyrolysis and its application in a diesel engine, *Fuel Process. Technol.*, vol. 92, no. 5, pp. 1129–1135, 2011,

[29] S. Frigo, M. Seggiani, M. Puccini, and S. Vitolo, Liquid fuel production from waste tyre pyrolysis and its utilisation in a Diesel engine, *Fuel*, vol. 116, pp. 399–408, 2014,

[30] M. Karagöz, Ü. Ağbulut, and S. Sarıdemir, Waste to energy: Production of waste tire pyrolysis oil and comprehensive analysis of its usability in diesel engines, *Fuel*, vol. 275, p. 117844, 2020,

[31] M. Chwist, K. Grab-Rogaliński, and S. Szwaja, Pyrolysis oil combustion in the CI engine, *Combust. Engines*, vol. 179, no. 4, pp. 126–131, 2019,

[32] T. Sinigaglia, M. Eduardo Santos Martins, and J. Cezar Mairesse Siluk, Technological evolution of internal combustion engine vehicle: A patent data analysis, *Appl. Energy*, vol. 306, p. 118003, 2022,

[33] M. Mikulski, J. Hunicz, K. Duda, P. Kazimierski, T. Suchocki, and A. Rybak, Tyre pyrolytic oil fuel blends in a modern compression ignition engine: A comprehensive combustion and emissions analysis, *Fuel*, vol. 320, p. 123869, 2022,

[34] P. Kasprzyk, J. Hunicz, A. Rybak, M. S. Gęca, and M. Mikulski, Excess Air Ratio Management in a Diesel Engine with Exhaust Backpressure Compensation, *Sensors*, vol. 20, no. 22, p. 6701, 2020,

[35] G. F. Hohenberg, Advanced approaches for heat transfer calculations, *SAE Tech. Pap.* 790825, 1979,

[36] S. Kline and F. McClintock, Describing Uncertainty in Single Sample Experiments, *Mech.*

*Eng.*, vol. 75, pp. 3–8, 1953.

[37] A. Maiboom, X. Tauzia, and J. F. Hétet, Experimental study of various effects of exhaust gas recirculation (EGR) on combustion and emissions of an automotive direct injection diesel engine, *Energy*, vol. 33, no. 1, pp. 22–34, 2008,

[38] M. Sjöberg, J. E. Dec, and W. Hwang, Thermodynamic and Chemical Effects of EGR and Its Constituents on HCCI Autoignition, *SAE Tech. Pap.* 2007-01-0207, 2007,

[39] A. C. Johansson, R. Molinder, T. Vikström, and H. Wiinikka, Particle formation during suspension combustion of different biomass powders and their fast pyrolysis bio-oils and biochars, *Fuel Process. Technol.*, vol. 218, p. 106868, 2021,

[40] J. Hunicz, J. Matijošius, A. Rimkus, A. Kilikevičius, P. Kordos, and M. Mikulski, Efficient hydrotreated vegetable oil combustion under partially premixed conditions with heavy exhaust gas recirculation, *Fuel*, vol. 268, p. 117350, 2020,

[41] T. Kitamura, T. Ito, J. Senda, and H. Fujimoto, Mechanism of smokeless diesel combustion with oxygenated fuels based on the dependence of the equivalence ration and temperature on soot particle formation, *Int. J. Engine Res.*, vol. 3, no. 4, pp. 223–248, 2002,

[42] J. Hunicz, M. Mikulski, P. C. Shukla, and M. S. Gęca, Partially premixed combustion of hydrotreated vegetable oil in a diesel engine: Sensitivity to boost and exhaust gas recirculation, *Fuel*, vol. 307, p. 121910, 2022,

[43] B. Rajesh Kumar, S. Saravanan, D. Rana, and A. Nagendran, Combined effect of injection timing and exhaust gas recirculation (EGR) on performance and emissions of a DI diesel engine fuelled with next-generation advanced biofuel – diesel blends using response surface methodology, *Energy Convers. Manag.*, vol. 123, pp. 470–486, 2016,